Ultra-Wideband Radar Based Sensing of Dielectric Material for Estimation of Boundaries

Taniya Das∗, Smriti Rani†, Anwesha Khasnobish‡, Arijit Chowdhury § , Tapas Chakravarty¶and Arpan Pal ‖

TCS Research

Email: (∗das.taniya, †smriti.rani,‡anwesha.khasnobish,§arijit.chowdhury2,¶tapas.chakravarty, ‖arpan.pal) @tcs.com

***Abstract*—The prime necessity for soil quality assessment using ultra wideband (UWB) radars is to characterize the soil layers with varying dielectric properties. Pre-requisite for such scenarios is determining soil layer boundaries and their respective dielectric properties. Towards that attempt, for the first time, this work introduces a technique to calculate the anterior and posterior boundary of a dielectric medium, with the help of a single monostatic UWB radar. Since soil consists of a large proportion of water with electrolyte, we validate our technique via experiments on potable water and salty water. The root mean squared error for anterior and posterior boundary detection is less than 0.13m and 0.40 m, respectively.**

***Index Terms*—boundary detection, dielectric, monostatic radar, precision agriculture, smart farming, soil quality assessment, UWB radar**

I. Introduction

Recent developments in smart farming and precision agriculture has called for a robust mechanism for micro level measurement of soil salinity and thereafter its change with conditions such as water evaporation, plant water intake, growing roots, among several others [1], [2]. Indirect methods of remote sensing help in monitoring such conditions continuously and for a long time. A portable hand held device can help farmers, hydrologists, agronomists in such scenarios as well. Furthermore, using back scattered radar signals to determine the dielectric properties and in turn soil moisture and salinity has shown potential [3]. Among radars, non-ionizing ultrawide band (UWB) radars provide good range and time resolution and are tissue penetrating [4]. Hence, ultrawide band imaging techniques are being explored vigorously for such use cases.

UWB radars are short-pulsed systems, which send a train of short duration pulses and analyse the echoed signal. The power spectral density of the transmitted signal is widespread across frequency spectrum and lower than noise floor of narrow band systems [5]. These systems work well in multi-path interference and have little energy consumption and are immune to multipath fading [6].

Due to these salient features, UWB radars can efficiently work as portable solutions for soil health measurement. Recent advances have seen UWB radar being used to estimate soil moisture and its pH levels using Fuzzy logic [2], channel impulse response (CIR) [7], maximum likelihood function estimation (MLE) [8]. Pre-requisite of any ultra-wideband real time imaging technique is boundary (anterior and posterior boundary) detection, i.e., where the electromagnetic (EM) waves enter and exit respectively from one dielectric medium to another. Secondly, if we retrieve the dielectric constant of a material under test, we can easily differentiate materials and in turn soil layers based on the dielectric constant.

Although researchers have uniquely tried to solve this problem by using various methods such as spectral analysis [9], [10] and many more, most of the advancement has been seen for ground penetrating radar [11], [12]. By traditional air radar system conventions, GPRs are effectively broadband [13], i.e. they have bandwidth (BW) in MHz. UWB radars, with their BW in GHz range, provide better resolution and are also have reduced interference from passive effects such as mist, aerosol, rain [14]. To the best our knowledge, we are first to use a monostatic UWB radar for estimation of boundaries of a dielectric medium.

Towards that effort, this paper, for the first time, presents a technique to calculate the boundary (both anterior and exterior), of a dielectric medium, using range-time matrix obtained from a monostatic UWB radar unit. Additionally, if physical parameters related to the dielectric material (anterior boundary, posterior boundary and dimension of dielectric medium container) are known, the relative dielectric constant of the material can be computed. This, as a first step towards microwave based material property investigation will be highly useful in measuring the effective dielectric constant for characterizing different soil layers. Since different soil layers have different dielectric constants, for validation of our technique, we have experimented with a plastic container filled with portable water and salty water, serving as different dielectric mediums.

The paper is organised as follows. Section II has information about the UWB radar and the experimental setup. It is followed by Section III, which contains the proposed signal processing algorithms used for finding entry and exit points from the obtained radar signal and related discussions. Results are analysed in Section IV and concluded in Section V.

II. Experimental Paradigm

A. Radar specification

All the experiments have been performed using Humatics'P440 Monostatic Radar Module [15] [16], as shown in Fig1. It is a mobile UWB radar with operating frequency lying between 3.15 to 4.8 GHz. It operates on precise time measurement (using two way time of flight).

The radar module provides output raw data in the form of a intensity valued fast time - slow time matrix, where the fast time axis or range axis is programmable to the desired range of visibility (RoV). For the experiments performed in this paper, we have used RoVs 2.63 m(N= 288 samples) and 3.51 m(N= 480 samples) [17] [18]. Slow time and fast sampling

frequency are 7.19 Hz and 16.4GHz respectively. Approximately 100 time samples were collected. Increasing number of samples will result in less noise in averaged signal, however it will increase the amount to time taken to complete the measurement. Moreover, experimental environment will also affect the signal noise level and hence number of samples should be increased/ decreased according to the environment. In our case, 100 samples were optimal in terms of time taken for experiments and accuracy results obtained.

Fig. 1: Humatics' P440 Monostatic UWB Radar Module

Distance resolution is 0.0091 m. Distance is synonymous with bin number (N). Our calculations are done with reference to bin numbers and later mapped to distance (in m) using equation 1.

$$1bin \sim 0.0091m \tag{1}$$

B. Experiment Design

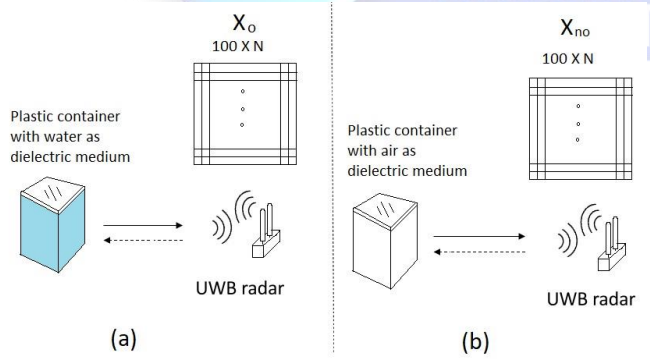

Fig. 2: Block diagram of Experimental Setup (a) With dielectric medium kept in front of the radar. (b) With air as medium.

As can be seen from Fig 2, the experiments have been performed using a plastic (PET, dielectric constant of 3.2) container filled with appropriate dielectric medium as the Object Under Test (OUT). The container has dimension of $0.18m \times 0.19m \times 0.23m$. The thickness of the plastic container is 2 mm. As the dielectric constant of PET plastic is very less than that of water ($\varepsilon r \approx 80$), so it is not considered for the rest of the analysis.

An air filled empty container is used as a background for reference. We have first tested our algorithm with water at room temperature ($\varepsilon r \approx 80$) as the dielectric medium [19]. Then we test it on another medium of 1 Molar aqueous solution of NaCl. Theoretically, its dielectric constant is $\varepsilon r \approx 70$ as given in [20]. In future works, we plan to replace the plastic container with appropriately designed human phantom.

Anterior and posterior boundary, when measured, are referred as entry and exit points/ distances respectively, in the paper signifying where the electromagnetic wave enters and exits the OUT. Both the terms have been used interchangeably.

III. Methodology

A. Algorithm for Anterior and Posterior Boundary Detection

Firstly, we collect 100 scans of data, when air is present as a dielectric medium (Fig. 2b). This data is called as background reference scans (X_{no}). It has a size of $100 \times N$, where N = number of samples per scan. Now, OUT scan data, X_o is collected, when the dielectric body (potable or salty water) is kept in the RoV (Fig. 2a). Size of X_o is also $100 \times N$. This is done so as to compare radar return at different distances with the background reference. A sharp difference is expected at the boundaries of the OUT with respect to background due to change of dielectric medium. Scans for both OUT(X_o) and background reference(X_{no}) are pre-processed to generate SignalS^a. S^a is further processed using the mentioned algorithm to find anterior boundary. Using S^a and anterior boundary range bin, signal S^b is calculated. Using the signalS^b, the same algorithm is used to find posterior boundary.

Fig 3 outlines the algorithm used to find distance of the anterior and posterior boundary from the radar.

1) Pre-processing: For pre-processing, mean of X_{no} and X_o is calculated and the absolute of the difference of the two is referred as signal S^a. Signal S^a has a size of $1 \times N$. Fig 4(a) shows an example plot of S_a for which OUT was kept at 0.42 m from the radar.

$$S_{1i}^a = |\sum_{j=1}^{100} X_o - \sum_{j=1}^{100} X_{no}|, \qquad i \in \{1,2,\ldots.N\} \tag{2}$$

2) Anterior Boundary Calculation: Here, the signal (S^a) received from equation 2 is processed further.

Step 1 For each i^{th} bin, Signal S^a is divided into 2 sub signals S_{1i}^a and S_{2i}^a , shown by equation (3).

$$S_{1i}^a = S^a(1:i) and\ S_{2i}^a = S^a(i+1:N), \quad \text{where } i \in \{2,\ldots.N-2\} \tag{3}$$

Step 2 Difference between standard deviation (σ) of SignalsS_{1i}^a andS_{2i}^a is calculated. This signal is called P^a.

$$P_i^a = \sigma(S_{1i}^a) - \sigma(S_{2i}^a), where\ i = 2\ to\ N-2 \quad (4)$$

If we take the difference of the standard deviation of the two signals S_{1i}^a and S_{2i}^a, we can expect a higher mismatch at the boundary of the dielectrics. These sharp differences can be detected well from P^a.

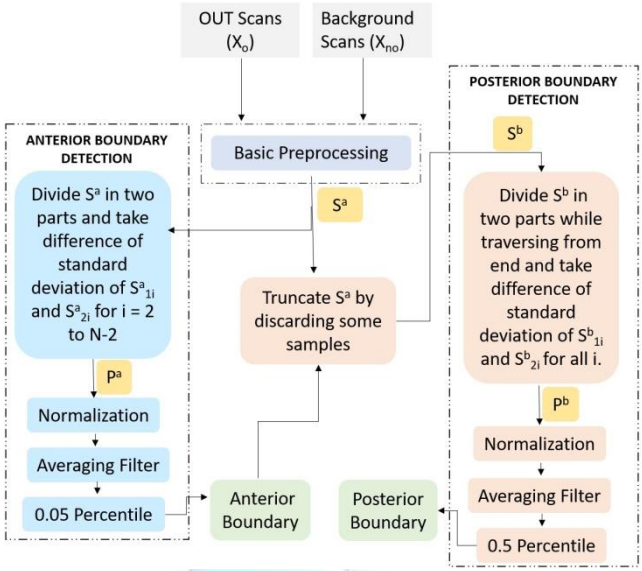

Fig. 3: Algorithm for estimating anterior and posterior boundary distance of OUT from radar.

Step 3 Signal P^a is normalised, using equation (5) and a 25-sample moving average filter is applied to it. The resultant P^a is depicted in Fig 4(b).

$$P^a(i) = \frac{P^a(i) - min(P^a)}{max(P^a) - min(P^a)} \quad (5)$$

Step 4 We calculate the percentile of P^a vector between its maximum and minimum bin number. Percentile values ranging from 0.05^{th} to 0.3^{th} are used to find their corresponding bin numbers. These detected bin numbers are converted to distance (in m) which corresponds to different boundary distances. These distances at different percentile values are tabulated and error in distance is analysed by comparing with known boundary value. Tabulation is presented in section IV and is used to find the optimal value of percentile for anterior boundary distance calculation.

Therefore, bin number (denoted by a) corresponding to optimal percentile value gives the output anterior boundary, referred as R_{entry}.

$$R_{entry} = a \times 0.0091m \quad (6)$$

where 0.0091 is multiplied to convert bin number to distance in 'metre'.

The range bin corresponding to the minimum value of P^a is very sensitive and prone to outliers. Hence, we have used percentile to determine boundary bin number.

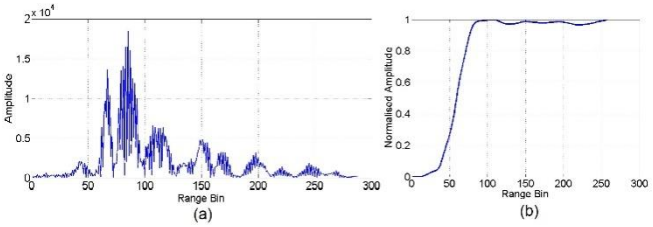

Fig. 4: Plots for anterior boundary detection for OUT kept at 0.42 m from radar. The x-axis corresponds to bin number while the y-axis gives the amplitude of the reflectance intensity of the signal plotted. (a)Signal S^a(b)Signal P^a

3) Posterior Boundary Calculation: After R_{entry} is calculated, samples are removed from S^a, starting from 1^{st} bin upto till detected anterior boundary bin number. This is done to remove portion of signal containing anterior part of the OUT. The signal is further flipped and truncated to get S^b of length n, where $n = N - \frac{R_{entry}}{0.0091}$. Fig 5(a) shows an example plot of S^b for which OUT was kept at 0.42 m from the radar.

Now, steps 1 to 4 in section III-A2 is repeated by replacing signal S^a with signal S^b for posterior boundary calculation. Step 3 gives P^b, as shown in Fig 5(b).

In step 4, percentile values through 0.25 to 0.75 are used and corresponding distances obtained are tabulated and analysed by comparing with actual posterior boundary distance. The table is used to find the optimal percentile value and the corresponding bin number. Let this bin number is b. Since the signal S^b is a flipped version of signal S^a, hence the posterior boundary distance is given by

$$R_{exit} = (n - b) * 0.0091m \quad (7)$$

Where, 0.0091is multiplied to convert bin number to distance in 'metre'.

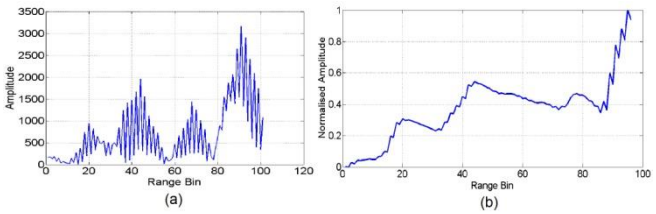

Fig. 5: Plots for posterior boundary detection for OUT kept at 0.42 m from radar. The x-axis corresponds to bin number while the y-axis gives the amplitude of the reflectance intensity of the signal. (a)Signal S^b (b) Signal P^b.

As can be seen from Fig, 4 and 5, considerable difference in P^a and P^b is observed at the boundary of the dielectric medium change.
Although after measuring anterior boundary distance, the actual (physical) posterior boundary will occur at

$$Physical\ Posterior\ Boundary = Anterior\ Boundary\ Distance + Width\ of\ OUT \quad (8)$$

However, in terms of radar return scan values, the posterior boundary will come at much later bin/distance, because speed of wave changes in dielectric medium other than air. For dielectric medium such as water or NaCl solution, speed to wave decreases inside it and hence posterior boundary distance will come at much later distance as compared to physical boundary. This is elaborated further in Section III-B.
Further, any mention of posterior boundary distance in this work is actually the bin number at which the wave exits the OUT, considering change of speed of wave inside the dielectric medium.

B. Apparent shift in Posterior Boundary

The OUT is kept at different distances ranging from 0.15 m to 1.0 m at different orientations, so that the width of OUT varies from 0.18 m to 0.23 m, and is used to determine the anterior and posterior boundary points. The calculations are done as follows:

Let the OUT is filled with a material having dielectric constant of ε_r, and kept at distance d_1 from radar antenna.

Since, $\varepsilon_r = 1$ for air medium, velocity of wave inside air as dielectric medium is $v = \frac{c}{\sqrt{1}} = c\ m/s$, where $c = 3 \times 10^8 m/s$. Hence, known $anterior\ boundary\ distance = c \times t = d_1\ m$, where t = time in sec. Further, physical width of $OUT = w\ m$. The dielectric slab is present inside OUT. Hence the time taken by wave to travel through the width w of the OUT is

$$\frac{w}{v} = \frac{w}{\frac{c}{\varepsilon_r}} = \frac{w \times \sqrt{\varepsilon_r}}{c} \quad (9)$$

This time is same if the wave passes through vacuum of width $w \times \sqrt{\varepsilon_r}$ in vacuum.

So, the known posterior boundary distance is:

$$\text{Known Posterior Boundary Distance} = \text{d1} + (w \times \sqrt{\varepsilon_r}) \quad (10)$$

For Example: Let the OUT is filled with water and kept at0.70 m from radar antennas. Hence,

- Known Anterior Boundary Distance =0.70 m.
- Dielectric constant $\varepsilon r = \sqrt{80}$.
- Width of dielectric slab = $0.18 \times 80\ m \approx 1.60m$.
- Known Posterior Boundary Distance $= 0.70 + 1.60\ m = 2.30m$

Alternatively, this developed algorithm can be used to approximate the dielectric constant of an unknown medium. If dimension of the OUT along with the physical anterior and posterior boundary distances from the radar antenna are known, we can use equation (10) to calculate ε_r of the dielectric medium present inside OUT.

All the ground truth (known) values for anterior and posterior boundary distances used for experiments are summarized in Table I. The anterior distance of OUT from radar was measured physically, while the known posterior boundary reported is the theoretically calculated posterior boundary using equation 10.

Here Both the radar module (P440) and OUT was kept at a constant height from the ground while performing the experiments.

TABLE I: Ground truth for anterior and posterior boundary

Dielectric Medium	**Water in OUT**					**1 M NaCl inOUT**		
Anterior Boundary (m)	0.15	0.42	0.6	0.7	0.96	0.6	0.8	1
Posterior Boundary (m)	1.75	2.02	2.65	2.3	2.56	2.1	2.3	2.5

The anterior distance measured above is actually the distance which is sending out minimum radiation due to low surface area. Since the radar receives radiations from every part from the frontal surface of the object, so the actual anterior and posterior boundary distances vary slightly from the measured. We have simulated a surface similar in dimension to the OUT and have scattered 10000 random points on it, to demonstrate this concept. Measuring each distance and plotting its probability density function (pdf), the actual anterior and posterior boundary points are determined. The mean or median of all possible computed distances, calculated from pdf plot, can be taken as the actual distances. All these findings are summarized in Table II.

TABLE II: Comparison of measured and simulated anteriorposterior boundary distances

Measured Entry (in m)	Simulated Entry (in m)		Measured Exit (in m)	Simulated Exit (in m)	
	Mean	Median		Mean	Median
0.42	0.43	0.43	2.02	2.02	2.02
0.70	0.70	0.70	2.30	2.30	2.30
0.15	0.17	0.17	2.56	2.56	2.56
0.96	0.96	0.96	1.75	1.76	1.76
0.60	0.61	0.601	2.65	2.65	2.65

IV. RESULTSAND DISCUSSION

The algorithm in section III-A is tested on OUT filled with two dielectrics, water at room temperature and 1 Molar aqueous NaCl solution. The results are analysed and compared by calculating RMS error and standard deviation of absolute error.

From the normalised P^a and P^b curve in Fig 4(b) and 5(b), to find the anterior boundary, we have to pinpoint at a particular value. For that purpose, different percentile in between the minimum and maximum levels are used to find the approximate distance. Different percentile such as 0.9,0.8,0.75,0.5,0.25,0.2,0.175,0.15,0.125,0.1,0.05 are used and compared with ground truth (known) boundary distance values to find the optimal percentile value.

A. Performance Analysis of Anterior Boundary Detection

Table III summarizes some of the percentiles which were used to detect anterior boundary with water as dielectric medium. As we can see, when the measured distance is 0.60 m, the closet value of detected entry point (anterior boundary), using our algorithm is 0.62 m at 0.05 percentile, in which case the absolute error is 0.02 m.

TABLE III: Anterior Boundary Detection

Percentile →	**0.05**	**0.1**	**0.125**	**0.05**	**0.1**	**0.125**
Measured Entry (in m)	**Detected Entry (in m)**			**Error(in m)**		
0.15	0.26	0.28	0.28	0.11	0.13	0.14
0.42	0.39	0.43	0.46	0.02	0.02	0.04
0.6	0.62	0.66	0.68	0.02	0.06	0.08
0.7	0.71	0.75	0.76	0.018	0.05	0.06
0.96	1.11	1.16	1.19	0.15	0.20	0.23

The entire result for anterior boundary detection is summarized in Fig 6 where RMS error is plotted against various percentiles, for both the dielectrics used. It can be pointed out that the RMS error is least at 0.05 percentile for both anterior and posterior distances. Hence it is chosen as the optimal percentile value.

The RMS error in anterior boundary distance calculation for water medium is 0.08 m while for NaCl solution it is 0.12 m. This shows that the algorithm works well in detecting anterior boundary of the plastic container.

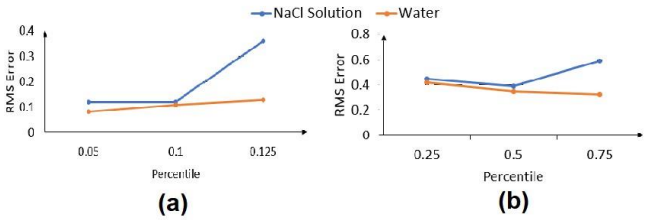

Fig. 6: (a) Error Analysis for Anterior Boundary (b)Error Analysis for Posterior Boundary

B. Performance Analysis of Posterior Boundary Detection

Similar to anterior boundary detection, the algorithm in section III-A3 is tested on OUT filled with two dielectrics, water at room temperature and aqueous NaCl solution. Posterior boundary is calculated using the equation 10. The results from posterior boundary detection are summarised in Fig 6 where we have plotted RMS error with percentiles used. As we can see, the minimum error is obtained at 0.5 percentile and hence it is chosen as the optimal percentile value. An RMS error of 0.35 m and 0.39 m is received from water and NaCl as dielectric, respectively, for posterior boundary distance calculation. So, we can say that algorithm for posterior boundary detection also performs reasonably well.

Results from analysis of both anterior and posterior boundary detection is tabulated in Table IV. We have used 0.05 and 0.5 percentile values for anterior and posterior detection respectively, as it was giving the best possible result. As, we can see for anterior boundary detection with water as dielectric medium, an RMS error of 0.08 m with standard deviation of 0.06 m is obtained. For NaCl solution RMS Error is 0.12 m with standard deviation of 0.11 m. Similarly for posterior boundary detection, water produces an RMS error of 0.35 m with standard deviation of 0.2 m while NaCl produces RMS error of 0.39 m with standard deviation of 0.27 m.

Further, we can say that our algorithm performs reasonably well, though posterior boundary detection is not at par with the anterior. This is because major portion of the UWB wave is reflected by the front part of the OUT and hence power of reflection for the rear end decreases sharply. This results in low magnitude of change at the posterior boundary of dielectric and hence is prone to more error.

TABLE IV: RMS Error and Standard Deviation for Anterior and Posterior Boundaries

	Dielectric Material	**RMS Error (in m)**	**Standard Deviation of Absolute Error (in m)**
Entry	Water	0.08	0.06
	NaCl	0.12	0.11
Exit	Water	0.35	0.2
	NaCl	0.39	0.27

V. CONCLUSIONAND FUTURE WORK

It can be said that using UWB scans, we can successfully detect anterior and posterior boundaries of the OUT filled with some dielectric material. The RMS error received for

anterior and posterior boundary distance measurement, for water and NaCl solution are 0.08 m, 0.35 m and 0.12 m, 0.39 m, respectively. This indicates that for a OUT with known dimension we can infer the dielectric constant by physically measuring the anterior and posterior boundaries and comparing it with the dimension of the known OUT. This work serves as the 1st step towards material property assessment, especially soil, where knowing the anterior-posterior boundary conditions for different dielectrics will be needed. This is a stepping stone towards soil health monitoring where the next step will be composition testing for unknown dielectric material mixture.

REFERENCES

[1] S. Kaundinya, E. Arnold, F. Rodriguez-Morales, and A. Patil, "A uasbased ultra-wideband radar system for soil moisture measurements," in 2018 IEEE Radar Conference (RadarConf18). IEEE, 2018, pp. 0721– 0726.

[2] J. Liang and F. Zhu, "Soil moisture retrieval from uwb sensor data by leveraging fuzzy logic," IEEE Access, vol. 6, pp. 29846–29857, 2018.

[3] W. Wu, A. S. Muhaimeed, W. M. Al-Shafie, and A. M. F. Al-Quraishi, "Using radar and optical data for soil salinity modeling and mapping in central iraq," in Environmental remote sensing and GIS in Iraq. Springer, 2020, pp. 19–40.

[4] R. O. R. Jenssen, M. Eckerstorfer, and S. Jacobsen, "Drone-mounted ultrawideband radar for retrieval of snowpack properties," IEEE Transactions on Instrumentation and Measurement, vol. 69, no. 1, pp. 221– 230, 2019.

[5] C. N. Paulson, J. T. Chang, C. E. Romero, J. Watson, F. J. Pearce, and N. Levin, "Ultra-wideband radar methods and techniques of medical sensing and imaging," in Smart Medical and Biomedical Sensor Technology III, vol. 6007. International Society for Optics and Photonics, 2005, p. 60070L.

[6] C.-C. Chiu, C.-H. Chen, S.-H. Liao, and T.-C. Tu, "Ultra-wideband outdoor communication characteristics with and without traffic," EURASIP Journal on Wireless Communications and Networking, vol. 2012, no. 1,p. 92, 2012.

[7] Q. Liang, B. Zhang, and X. Wu, "Gulf of mexico oil spill impact on beach soil: Uwb radars-based approach," in 2012 IEEE Globecom Workshops. IEEE, 2012, pp. 1445–1449.

[8] M. Liu, F. Zhu, and J. Liang, "Channel modeling based on ultra-wide bandwidth (uwb) radar in soil environment with different ph values," in 2014 Sixth internationalconference on wireless communications and signal processing (WCSP). IEEE, 2014, pp. 1–6.

[9] D. O. Batrakov, M. S. Antyufeyeva, A. V. Antyufeyev, and A. G. Batrakova, "Inverse problems and uwb signals in biomedical engineering and remote sensing," in 2016 8th International Conference on Ultrawideband and Ultrashort Impulse Signals (UWBUSIS). IEEE, 2016, pp.148–151.

[10] G. P. Pochanin, V. P. Ruban, A. G. Batrakova, S. N. Urdzik, and D. O. Batrakov, "Measuring of thickness of the asphalt pavement with use ofgpr," in 2014 15th International Radar Symposium (IRS). IEEE, 2014, pp. 1–4.

[11] K. Zaj´ıcova and T. Chuman, "Application of ground penetrating radar´ methods in soil studies: A review," Geoderma, vol. 343, pp. 116–129, 2019.

[12] A. Klotzsche, F. Jonard, M. C. Looms, J. van der Kruk, and J. A. Huisman, "Measuring soil water content with ground penetrating radar: A decade of progress," Vadose Zone Journal, vol. 17, no. 1, pp. 1–9, 2018.

[13] A. Benedetto and F. Benedetto, "Application field–specific synthesizing of sensing technology: Civil engineering application of groundpenetrating radar sensing technology," 2014.

[14] I. I. Immoreev and P. D. V. Fedotov, "Ultra wideband radar systems: advantages and disadvantages," in 2002 IEEE Conference on Ultra Wideband Systems and Technologies (IEEE Cat. No. 02EX580). IEEE, 2002, pp. 201–205.

[15] "The humatics p440 development module," https://humatics.com/industries/research-and-education/humaticsradar-kit/.

[16] A. Chowdhury, T. Das, S. Rani, A. Khasnobish, and T. Chakravarty, "Activity recognition using ultra wide band range-time scan."

[17] "P440 documentation," https://humatics.com/resources/.

[18] "Humatics," https://humatics.com/.

[19] D. G. Archer and P. Wang, "The dielectric constant of water and debyehuckel limiting law slopes,"" Journal of physical and chemical reference data, vol. 19, no. 2, pp. 371–411, 1990.

[20] J. Hasted, D. Ritson, and C. Collie, "Dielectric properties of aqueous ionic solutions. parts i and ii," The Journal of Chemical Physics, vol. 16, no. 1, pp. 1–21, 1948.